

Investigation of Lithiation Mechanism of LiCr_3O_8 as Potential Anode Materials for Lithium-ion Batteries

Fei Li, Quanchao Zhuang*, Xiangyun Qiu, Zhi Sun

Li-ion Batteries Lab, School of Materials Science and Engineering, China University of Mining and Technology, Xuzhou 221116, China;

*E-mail: zhuangquanchao@126.com

Received: 2 January 2013 / Accepted: 8 February 2013 / Published: 1 March 2013

LiCr_3O_8 as a novel anode material for lithium ion batteries was prepared by a new liquid phase method. Its structure, morphology and electrochemical performance were characterized by X-ray diffraction (XRD), scanning electron microscopy (SEM), and constant current charge and discharge test. It was found that the lithiation process of LiCr_3O_8 in the initial discharge process contained two-steps, namely, the reduction of Cr^{6+} at a relatively high potential via lithium insertion reaction and the reduction of Cr^{3+} by means of conversion reaction at a low potential. However, the lithiation process of LiCr_3O_8 in the initial charge process and following charge and discharge cycles was similar to that of Cr_2O_3 . In addition, due to the existence of excess Li_2O , its cycle performance was more excellent than commercial Cr_2O_3 . To further investigate the electrochemical behavior of LiCr_3O_8 in the initial discharge process, electrochemical impedance spectroscopy (EIS) for LiCr_3O_8 electrode were obtained at different potentials. According to the results of equivalent circuit analysis, the change of kinetic parameters for lithiation process of LiCr_3O_8 as a function of potential in the first discharge cycle was discussed in detail.

Keywords: Lithium ion batteries; LiCr_3O_8 ; SEI film; EIS

1. INTRODUCTION

With the development of new energy technologies, rechargeable lithium ion batteries are becoming a key-enabling technology for electric vehicles and hybrid electric vehicles owing to their high energy densities [1]. Since the technological breakthrough of anode materials for lithium secondary battery in the end of 1980s and early 1990s resulting in the birth and commercialization of lithium ion battery, although research on a lot of anode materials has been a focus, to our knowledge, graphitic is still the dominant one available on the market due to excellent cycle performance [2]. However, for the increasing requirement of improving capacity of the power batteries, the limited

capacity of graphitic carbon (theoretically 372 mAh/g^{-1}) is gradually unable to meet the need and provides a motivation to develop new anode materials [3].

In 2000, Poizot et al. [4] reported that lithium can be stored reversibly in transition metal oxides (TMO) through a heterogeneous conversion reaction (where $\text{TM}=\text{Co, Fe, Ni, Cu, and so on}$), i.e. $\text{MO}_x + 2x\text{Li} \rightarrow \text{M}^0 + x\text{Li}_2\text{O}$, which was different from the intercalation/de-intercalation mechanism. Usually, reversible capacities in these systems, which has been demonstrated as innovative high energy anode materials for lithium-ion batteries, are in the range of 400-1100 mAh/g. Therefore, as potential alternatives for graphite, transition metal oxides attract lots of attention in recent years [4-12].

Among most of the transition metal (TM) oxides as anodes for Li-ion batteries, Cr_2O_3 is quite attractive due to its relative low electrochemical motive force value of 1.085 V vs. Li/Li^+ [13-14] and relative high reversible capacity of 800 mAh/g [14-15]. But the cycle performance of pristine Cr_2O_3 is very poor due to large volume expansion during the charge-discharge process, and it has not yet been commercialized [5]. Compared to Cr_2O_3 , LiCr_3O_8 will have much higher theoretical capacity than Cr_2O_3 , if it can achieve lithium storage through conversion reaction, for the reason that the average valence state of chromium in LiCr_3O_8 is +5, higher than that in Cr_2O_3 . Furthermore, the content of Li_2O in conversion reaction of LiCr_3O_8 is increased in comparison with Cr_2O_3 , and this will inhibit the volume variation caused by conversion reaction, thus improve its specific capacity and cycle performance as proposed and verified by Chen et al. [16-18].

Early in 1980s, there had been a few reports about electrochemical behavior of LiCr_3O_8 in the 1-4 V voltage range and its good resistance to high temperature, which can be used as cathode material for lithium ion batteries [19-20]. However, since then it had been rarely reported, probably due to the difficulty of its preparation. Furthermore, as to our knowledge, whether LiCr_3O_8 can achieve lithium storage through conversion reaction and be used as anode materials for lithium-ion batteries materials, are still unknown. Specially, if LiCr_3O_8 can achieve lithium storage through conversion reaction, what is the lithiation mechanism of LiCr_3O_8 ?

What is more, LiCr_3O_8 is always prepared by high-temperature solid-phase method, which is easy to produce sintering and agglomeration. Therefore, in our study, a new simple liquid phase method is developed to prepare LiCr_3O_8 in a relatively lower temperature, which can better control its crystallinity and morphology. The electrochemical performance and lithiation mechanisms of LiCr_3O_8 are investigated by charge-discharge test, and electrochemical impedance spectroscopy (EIS).

2. EXPERIMENTAL METHODS

Materials Preparation. LiCr_3O_8 was prepared by a simple liquid phase method. $\text{Li(OH)·H}_2\text{O}$ (Kelong Co. Chengdu, China) and $\text{Cr(NO}_3)_3·9\text{H}_2\text{O}$ (Guoyao Co. Beijing, China) (5% molar excess of Li was used) were mixed uniformly by ball milling for 2 hours. The as prepared sample was dispersed in deionized-water and uniformly stirred. Then the solution was sintering in air at 300 °C for 10 hours. After cooling down to room temperature naturally, the solid product was rinsed by deionized-water and dried at 40 °C for 10 hours.

X-ray Diffraction. The crystal structure was investigated by powder diffraction on a Rigaku D/Max-3B diffractometer equipped with a monochromatized Cu K α radiation source. Diffraction data were collected by step scanning over an angular range of 20–70° with a step width of 0.01° (35 KV, 30 mA). A scanning electron microscope (SEM, Hitachi, S-3000N) were used to investigate the morphology and size of the samples.

Electrochemical Characterization. The LiCr₃O₈ electrode were prepared by pasting a slurry composed of the active material (70 wt%), carbon black (Shanshan Co. Shanghai, China) (15 wt%) and polyvinylidene fluoride (PVDF) (Kynar FLEX 2801, Elf-atochem, USA) binder (15 wt%) in N-methylpyrrolidone (NMP) onto an copper foil current collector. As compared, the commercial Cr₂O₃ electrode was prepared using the same procedure. The electrolyte was 1 mol·L⁻¹ LiPF₆-EC:DEC:DMC (volume ratio 1:1:1, Guotaihuarong Co. Zhangjiagang, China). Testing cells were assembled in the glove box for evaluating the electrochemical performances of the materials.

Charge and discharge experiment was conducted in a 2025 coin cell using lithium metal as the second electrode. The cells were galvanostatically charged and discharged at a current density of 20 mA/g over a potential range between 0 and 3.0 V. Electrochemical impedance experiments were conducted in a three-electrode glass cell with Li foils as both auxiliary and reference electrodes using an electrochemical work station (CHI660D, Chenhua Ltd Co. Shanghai, China). The amplitude of ac perturbation signal was 5 mV and the frequency range was from 10⁵ to 10⁻² Hz. The impedance data were analyzed in Zview software.

3. RESULTS AND DISCUSSION

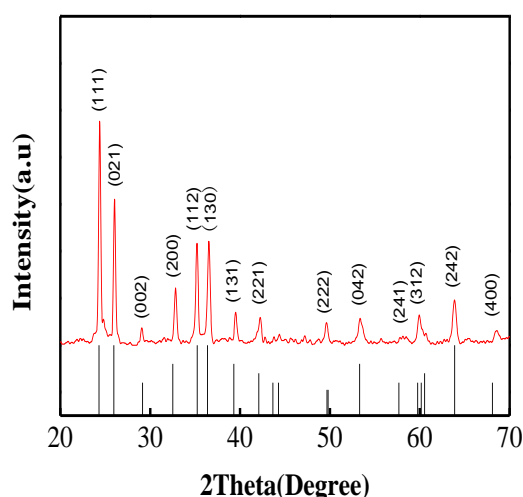


Figure 1. XRD patterns of LiCr₃O₈

Figure.1 shows the XRD patterns of LiCr₃O₈ samples. It can be seen that the diffraction peaks of LiCr₃O₈ prepared in this method are in good agreement with the PDF standard. Specially, the shape of the peaks is very sharp, indicating that LiCr₃O₈ sample has a good crystal structure.

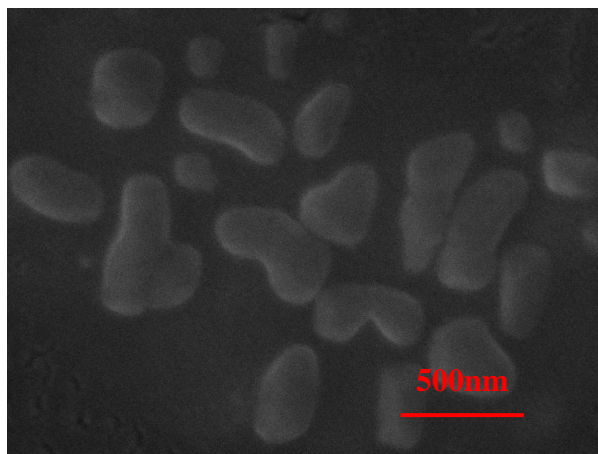


Figure 2. SEM image of LiCr₃O₈

Figure.2 shows a typical SEM of LiCr₃O₈ samples. It is obviously found that the particle morphology of LiCr₃O₈ sample is similar to “peanut shells” with an average size of 400 nm. Moreover, the majority of the particles sizes are uniform without sintering and agglomeration, indicating much better morphology of particles.

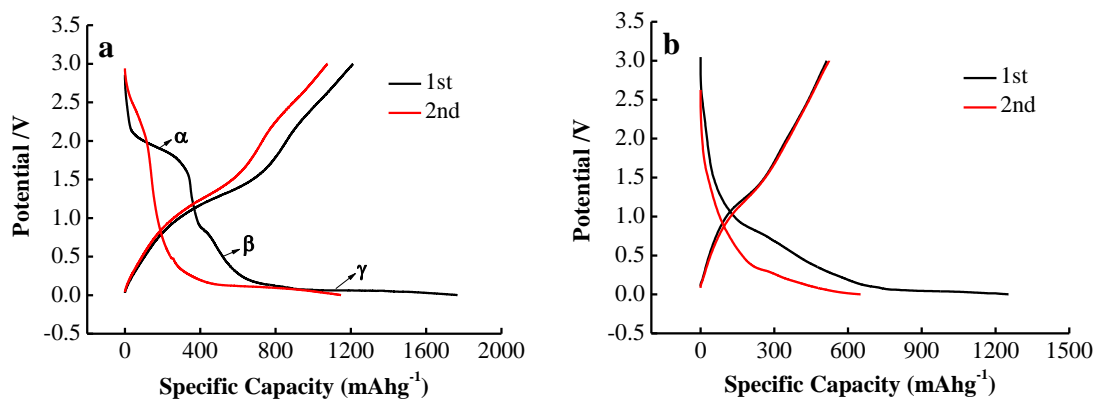
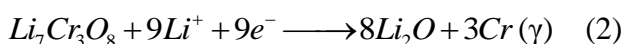


Figure 3. Charge-discharge curves of (a) LiCr₃O₈ and (b) commercial Cr₂O₃

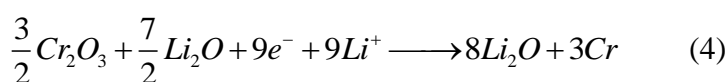
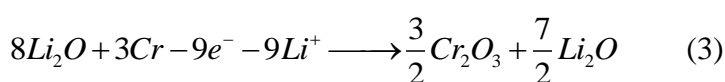
Typical discharge and charge curves of Li/LiCr₃O₈ cell in the range of 3.0-0.0 V are shown in Figure.3 (a). It can be seen that the initial discharge capacity of LiCr₃O₈ composite reaches 1766 mAh/g, and the first discharge curve is mainly composed of two plateaus (α, γ) located near 1.8 and 0.0 V, respectively, and a sloped region (β) near 0.8 V. It is well known that the structure of LiCr₃O₈ is composed of (Li, Cr)O₆ octahedra, which forms staggered strings by edge sharing in the direction of the c-axis, and CrO₄ tetrahedra which connects the octahedra strings to a three-dimensional framework by corner sharing. Each tetrahedron is in contact with three different strings. The lithium and chromium atoms are randomly distributed on the octahedral sites [21-22]. Due to the strong oxidizing property of Cr⁶⁺, with the decrease of the polarization potential, the high valence state of Cr will be reduced at first [20]. Therefore, the plateau α observed at 2.0 V provides a capacity of about 533

mAh/g, which shows that the total number of inserting lithium during this process is ca 6 Li per formula unit (consistent with the theoretical values of lithium ions intercalation) by calculation, corresponding to a complete reduction of the oxidation state of two chromium ions from 6 to 3, so the plateau α can be attributed to the formation of $\text{Li}_6\text{LiCr}_3\text{O}_8$, which is caused by lithium ions inserting into Cr-O tetrahedral as suggested by Koksang et al. [20]. The sloped region β near 0.8 V, which provides a capacity of 102 mAh/g and disappears in the second week, which corresponds to a generally accepted fact that the SEI film is formed near 0.8 V due to the decomposition of electrolyte solution species such as ethylene carbonate (EC) [23]. Thus the only explanation accounting for these observations is that the sloped region β is mainly due to the formation of the SEI film. With deeply discharging close to 0 V, the plateau γ appears and provides a capacity of 1131 mAh/g, which is much higher than the capacity when the number of inserting lithium is ca 9 Li per formula unit, indicating that Cr^{3+} has been completely reduced to metal Cr and the extra lithium storage capacity may be derived from interfacial lithium storage phenomena [24-26]. Therefore, the plateau γ can be ascribed to the formation of nano-composite phase ($\text{Li}_2\text{O}/\text{Cr}$) through conversion reaction and the interfacial lithium storage between the nano-phases.

According to the above results, it can be concluded that there are two different lithiation processes of LiCr_3O_8 , namely, the reduction of Cr^{6+} at a relatively high potential via lithium insertion reaction and the reduction of Cr^{3+} by means of conversion reaction at a low potential, and the first lithiation process of LiCr_3O_8 can be represented as follows:



It can further be seen that from Figure.3 (a) that the curve of LiCr_3O_8 electrode in the second discharge process is different from that in the first discharge process, namely, the plateau α completely disappears in the second discharge process, indicating the lithiation mechanism in the first discharge process is different from that in the second discharge process. The lithiation reaction product of LiCr_3O_8 is $\text{Li}_2\text{O}/\text{Cr}$ nanocomposite phase, which is the same as that of Cr_2O_3 . In addition, the first charge curve and the second charge-discharge curves of LiCr_3O_8 are similar to that of Cr_2O_3 (as shown in Figure.3 (b)). Moreover, the structure of LiCr_3O_8 had irreversibly broken down in the first discharge process, so it is difficult to recover [20]. Thus we assumed that $\text{Li}_2\text{O}/\text{Cr}$ nanocomposite phase is transformed into not LiCr_3O_8 but $\text{Cr}_2\text{O}_3/\text{Li}_2\text{O}$ nanocomposite phase probably due to the high valence state of LiCr_3O_8 , and in the following charge and discharge cycles the lithiation process of LiCr_3O_8 can be represented as follows:



The differential capacity curves of LiCr_3O_8 (a) and commercial Cr_2O_3 (b) are showed in Figure.4.

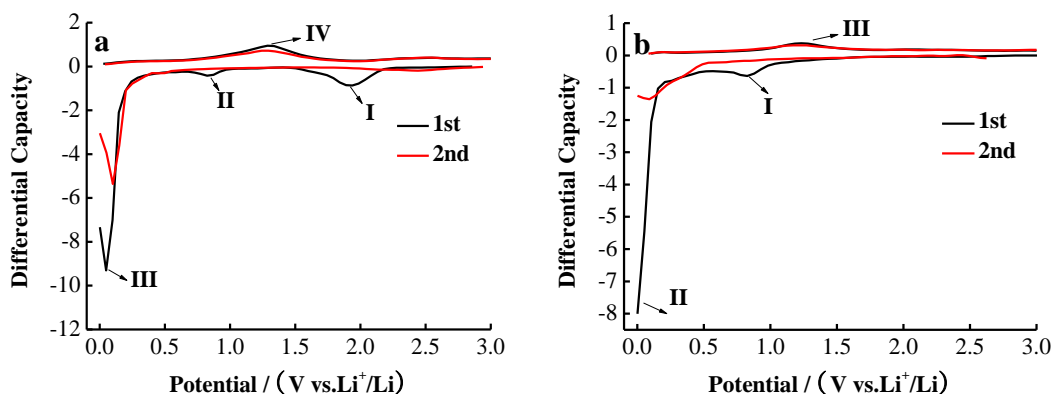


Figure 4. Differential capacity curves of (a) LiCr_3O_8 and (b) commercial Cr_2O_3

The voltage profile exhibits its electrochemical activity. It can be seen that three reduction peaks were clearly observed in the differential capacity curve of LiCr_3O_8 during the first discharge process, corresponding to three plateaux voltages in the first discharge curve. However, only two reduction peaks are observed in the differential capacity curve of Cr_2O_3 during the first discharge process, indicating that lithiation mechanism of LiCr_3O_8 in the first discharge process is different from that of Cr_2O_3 . One reduction peaks could be observed in the differential capacity curve of LiCr_3O_8 during the first charge process, which is similar to that of Cr_2O_3 . Furthermore, the differential capacity curve of LiCr_3O_8 during the second discharge process is almost identical to that of Cr_2O_3 , displaying that lithiation mechanism of LiCr_3O_8 in the first charge process and second charge-discharge process is the same as that of Cr_2O_3 , this further confirm our above assumption.

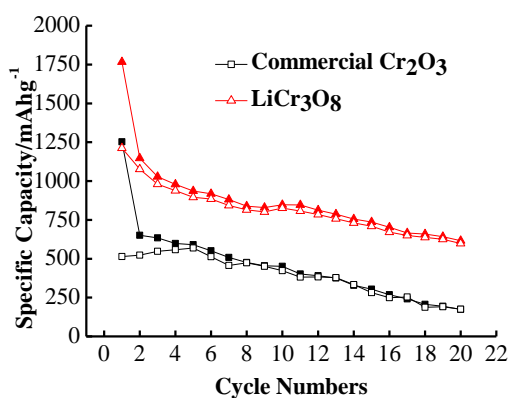


Figure 5. Cycle performance curves of LiCr_3O_8 and commercial Cr_2O_3

Figure.5 shows the cycle performance curves of LiCr_3O_8 and commercial Cr_2O_3 . It can be seen that the initial specific discharge and charge capacity of LiCr_3O_8 is 1766 mAh/g and 1212 mAh/g, respectively, and the initial coulomb efficiency of LiCr_3O_8 reaches about 68.6%, while the initial

specific discharge and charge capacity of commercial Cr_2O_3 is 1252 mAh/g and 513 mAh/g respectively, and the initial coulomb efficiency of commercial Cr_2O_3 reaches about 41.0%, which is lower than that of LiCr_3O_8 . After 20 cycles, the charge capacity of commercial Cr_2O_3 is 175 mAh/g, and its capacity retention is only 34.1%, while the charge capacity of LiCr_3O_8 is 598 mAh/g, and the capacity retention of LiCr_3O_8 is 49.3%, higher than that of commercial Cr_2O_3 . The above results show that the cycle performance of LiCr_3O_8 is much better than commercial Cr_2O_3 . Considering LiCr_3O_8 has transformed into $\text{Cr}_2\text{O}_3/\text{Li}_2\text{O}$ composite electrode in the initial discharge process, and Li_2O can not fully decomposed in the following charge process, namely, there exists excess Li_2O in the $\text{Cr}_2\text{O}_3/\text{Li}_2\text{O}$ composite electrode, which may contributes to inhibit dramatic conversion reaction and the volume change as suggested by Chen et al. [16-18], thus improve its cycle performance.

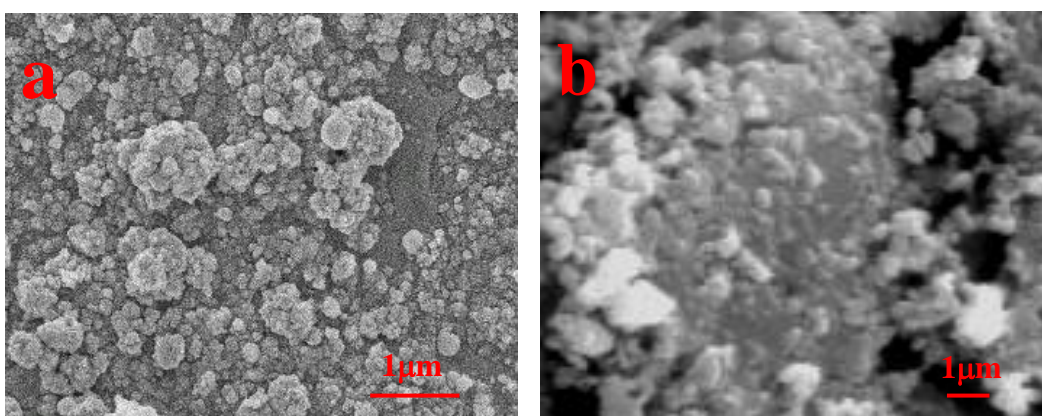


Figure 6. SEI image of (a) LiCr_3O_8 and (b) commercial Cr_2O_3 electrode at 0 V after the initial discharge process

Furthermore, it can be seen from Figure.6 that compared to Cr_2O_3 , much closer interface morphology of LiCr_3O_8 electrode with no obvious cracks is observed after the initial discharge process, indicating that LiCr_3O_8 electrode presents more stable interface characteristics, and the electronic contact between active particles is much better, further demonstrate that the excellent cycle performance LiCr_3O_8 is due to excess Li_2O in the $\text{Cr}_2\text{O}_3/\text{Li}_2\text{O}$ composite electrode.

To investigate lithium ion insertion mechanism at the electrode/electrolyte interface, EIS measurements are carried out for the LiCr_3O_8 electrode during the first charge and discharge cycle at room temperature. Figure.7 shows the Nyquist plots obtained from the LiCr_3O_8 electrode in the potential region from 2.8 V to 0.3 V during the first discharge process. It can be seen that, at open circuit potential 2.8 V, the Nyquist plots of LiCr_3O_8 electrode are mainly composed of three parts: a small semicircle in the high-frequency region (HFS), another small semicircle in the middle-frequency region (MFS) and a slightly inclined line in the low-frequency region. With the decrease of the electrode polarization potential, the HFS and MFS gradually begin to overlap each other, eventually turn into one semicircle. While the inclined line in the low-frequency region shows an increasing tendency to move towards the real axis, and another semicircle in the low frequency region (LFS) and a steep sloping line in the lower frequency region (LFL) is formed at 1.9 V corresponding to the

plateau in the voltage profile in the initial discharge curves, indicating that LFS and LFL should be ascribed to charge transfer step and solid state diffusion, respectively.

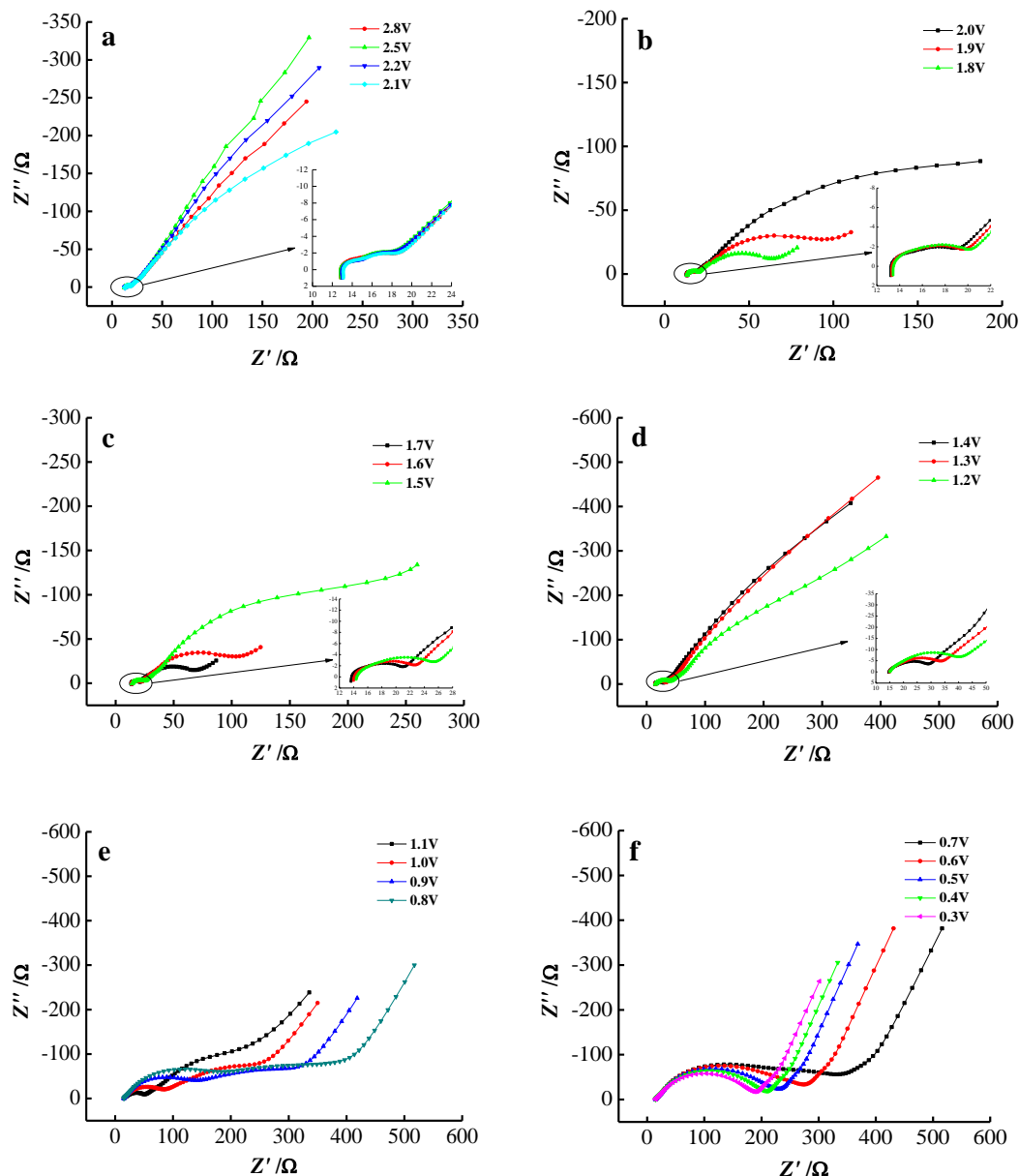


Figure 7. Impedance spectra of LiCr_3O_8 electrode at various potentials in the first discharge process (a) 2.8-2.1 V (b) 2.0-1.8 V (c) 1.7-1.5 V (d) 1.4-1.2 V (e) 1.1-0.8 V (f) 0.7-0.3 V

Thus the spectra in the first discharge process can be distinguished in four sections, namely HFS, MFS, LFS and LFL. In our previous studies, the processes of the first delithiation/lithiation of the spinel LiMn_2O_4 [27] and LiCoO_2 [28] electrode were investigated by EIS. Three semicircles, which are similar to that of LiCr_3O_8 electrode obtained in this study, were also observed in the Nyquist diagram at intermediate degrees of intercalation, and the three semicircles are attributed to the migration of lithium ions through the SEI films, the electronic properties of the material and the charge

transfer step, respectively. Therefore, three semicircles obtained in this study are also attributed to the migration of lithium ions through the SEI films, the electronic properties of the material and the charge transfer step, respectively.

Along with the decrease of the electrode polarization potential, LFS and LFL is transformed into an slightly inclined line at 1.4 V, displaying charge transfer proceeds hardly during those potentials. When the electrode potential is changed from 1.4 V to 1.1 V, the slightly inclined line in the low frequency region is evolved into LFS and LFL again, corresponding to the beginning of conversion reaction in the discharge curve, this further demonstrates that LFS should be ascribed to the charge transfer step undoubtedly. On further discharging to 0.3 V, the semicircle arising from overlapping each other of HFS and MFS and LFS begin to overlap each other at 0.8 V, and turn into one semicircle below 0.6 V.

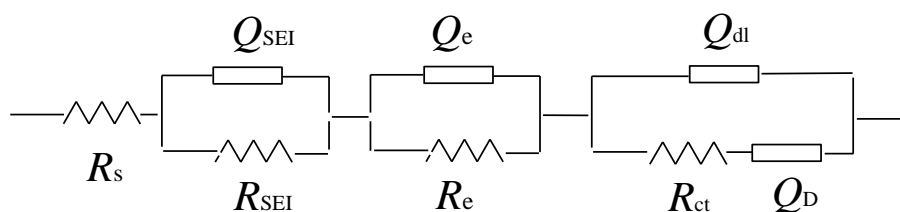


Figure 8. Equivalent circuit proposed for analysis of LiCr_3O_8 electrode in the first discharge process, R_s : ohmic resistance; R_{SEI} : resistances of SEI film; R_e : electronic resistance; R_{ct} : resistances of charge transfer reaction; Q_{SEI} : capacitance of SEI film; Q_e : capacitance of electronic resistance; Q_{dl} : capacitance of double layer; Q_D : capacitance of charge transfer reaction

According to the experimental results obtained in this work, a new equivalent circuit, as shown in Figure.8, is proposed to fit the impedance spectra of the LiCr_3O_8 electrode in the first discharge process. In this equivalent circuit, R_s represents the ohmic resistance, R_{SEI} , R_e and R_{ct} are resistances of the SEI, the electron and the charge transfer reaction. The capacitance of the SEI, the capacitance of electronic resistance and the capacitance of the double layer are represented by the constant phase elements (CPE) Q_{SEI} , Q_e and Q_{dl} , respectively. The low frequency region, however, cannot be modeled properly by a finite Warburg element. We have chosen, therefore, to replace the finite diffusion by a CPE, i.e. Q_D . This approach has been used to characterize the graphite electrode [29] and has allowed us to obtain a good agreement with the experimental data. The expression for the admittance response of the CPE (Q) is

$$Y = Y_0 \omega^n \cos\left(\frac{n\pi}{2}\right) + j Y_0 \omega^n \sin\left(\frac{n\pi}{2}\right), \quad (5)$$

Where ω is the angular frequency and j is the imaginary unit. A CPE represents a resistor when $n = 0$, a capacitor with capacitance of C when $n = 1$, an inductor when $n = -1$, and a Warburg resistance when $n = 0.5$.

Figure.9 shows variations of R_{SEI} with electrode potential obtained from fitting the experimental impedance spectra of LiCr_3O_8 electrode during the first discharge process. As is

obviously shown above, when the electrode polarization potential is changed from 2.8 to 2.0 V, the change of R_{SEI} is small, implying the change of the thickness of SEI film is not obvious.

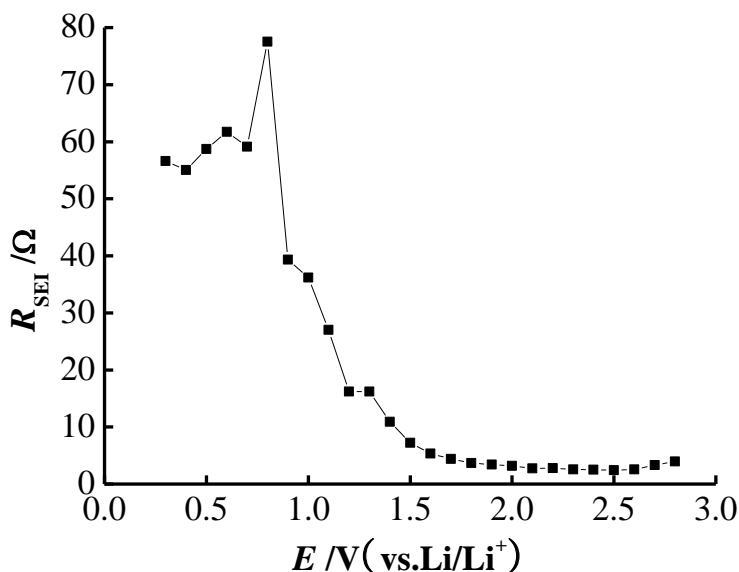


Figure 9. Variations of R_{SEI} with electrode potentials for LiCr_3O_8 in the first discharge cycle

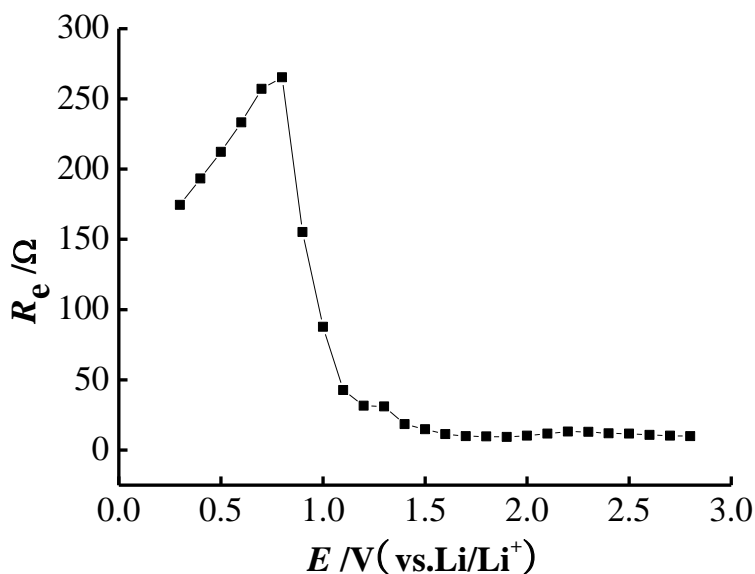


Figure 10. Variations of R_e with electrode potentials for LiCr_3O_8 in the first discharge cycle

On further discharging to 0.8 V, R_{SEI} slowly increases above 1.2 V, and then rapidly increases in the potential range between 1.2 and 0.8 V, signifying that SEI film is mainly formed in the above potential range, which further confirms that the sloped region β near 0.8 V in the initial discharge curve the formation of the SEI film. In the course of the subsequent discharge, from 0.8 V to 0.7 V, R_{SEI} decreases. It is probably due to that after the lithiation reaction, the components of the SEI film formed on the active material react with some impurities (such as trace water) in the electrolyte in the

aging process and generate some substances (such as Li_2CO_3), which promote the conduction of lithium ions, improve the uniformity of the SEI film and accelerate the migration of lithium ions between the electrode interface. Below 0.7 V, the change of R_{SEI} is not significant, indicating that the SEI film has been basically stable.

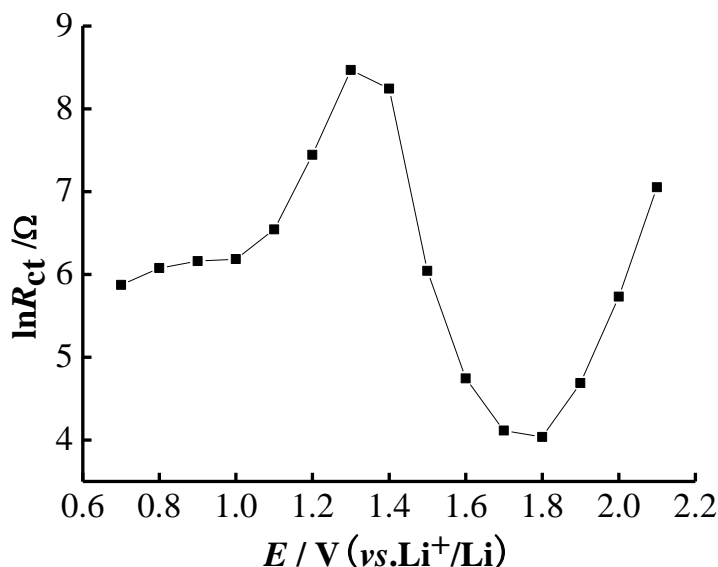


Figure 11. Variations of R_{ct} with electrode polarization potentials for LiCr_3O_8 electrode in the first discharge process

Variations of R_e obtained from fitting the experimental impedance spectra of the LiCr_3O_8 electrode during the first discharge cycle are shown in Figure.10. As can be seen, from 2.8 V to 1.1 V, R_e does not change significantly, indicating that the electronic conductivity of LiCr_3O_8 electrode keeps almost constant in the lithium intercalation process. However, on further discharging to 0.5 V, R_e slowly increases rapidly, displaying that the electronic conductivity of LiCr_3O_8 electrode decreases rapidly, which is obviously owing to that the active material and conductive agent separate from each other caused by the volume expansion of electrode in the conversion reactions and the volume expansion of active material itself will lead to lower electronic conductivity of the electrode. Below 0.8 V, R_e gradually decreases with the decrease of the electrode polarization, mainly due to that the formation of $\text{Li}_2\text{O}/\text{Cr}$ composite phase will increase the electronic conductivity of the electrode.

Variations of R_{ct} with the change of electrode polarization potential are shown in Figure.11, which reflects the difficulty of electrochemical reaction. The R_{ct} versus E plot is supposed to behave according to the following classical equation [30]:

$$R_{ct} = 1 / f F k_0 A c_O^{0.5} c_R^{0.5} \tag{6}$$

In this equation, f denotes the usual electrochemical constant (equal to F/RT with F and R being the Faraday and gas constant, respectively, and T the absolute temperature), and k_0 is the heterogeneous rate constant. Specially, the total concentration of available intercalation sites, c_T , is

constant, i.e., $c_O + c_R = c_T$. The concentration of the reduced form, c_R , and that of the oxidized form, c_O , are identified with the concentration of lithium ions and unoccupied intercalation sites, respectively. Equation 6 clearly predicts a rapid increase in R_{ct} as $c_O \rightarrow c_T$, $c_R \rightarrow c_T$, i.e., for either the completely intercalated or deintercalated states, and there is a minimum value of R_{ct} when c_O or c_R equals $c_T/2$. It can be clearly seen that with the decrease of electrode polarization potential, from 2.1 V to 1.3 V, R_{ct} shows a trend of first decrease and then increase, corresponding to the lithiated phase $\text{Li}_6\text{LiCr}_3\text{O}_8$ are formed in the first discharge process. The results confirmed that Equation 1 can be used to correctly interpret the experimental data. As a consequence, the semicircle in the low frequency is undoubtedly attributed to the charge transfer process. From 1.3 V to 0.7 V, R_{ct} appears to continuously decrease, displaying the beginning of conversion reaction.

4. CONCLUSIONS

In the present studies, LiCr_3O_8 was prepared by a new liquid phase method, its structure, morphology and electrochemical performance were characterized by XRD, SEM, and constant current charge and discharge test. In addition, the first lithiation process of LiCr_3O_8 electrode was investigated by EIS. The results illustrated that the lithiation process of LiCr_3O_8 in the initial discharge process contained two-steps, namely, the reduction of Cr^{6+} at a relatively high potential via lithium insertion reaction and the reduction of Cr^{3+} by means of conversion reaction at a low potential. However, the lithiation process of LiCr_3O_8 in the initial charge process and following charge and discharge cycles is similar to that of Cr_2O_3 . The initial specific discharge and charge capacity of LiCr_3O_8 is 1766 mAh/g and 1212 mAh/g, respectively, and the initial coulomb efficiency of LiCr_3O_8 reaches about 68.6%, which are both higher than that of Cr_2O_3 due to the existence of excess Li_2O in the lithiation products of LiCr_3O_8 which inhibited the dramatic conversion reaction and the volume change as confirmed by comparing the morphology of LiCr_3O_8 electrode after the initial discharge process with commercial Cr_2O_3 . The equivalent circuit simulation results revealed that, the decrease of electronic conductivity and the unstable SEI film of LiCr_3O_8 electrode may be the important reasons that led to the reduction of cycle performance of LiCr_3O_8 electrode. The current studies advance the view points of previous reported on the conversion reaction mechanisms in the literature, and would undoubtedly facilitate further the great progress of design and preparation of high property transition metal oxides for commercial application.

ACKNOWLEDGEMENTS

This work was supported by the Fundamental Research Funds for the Central Universities (2010LKHX03, 2010QNB04, 2010QNB05) and "Science and Technology Climbing Program" of China University of Mining & Technology (N090237).

References

1. J. Tollefson, *Nature*, 456 (2008) 436.

2. Y. P. Wu, C. Wan, C. Jiang, S.B. Fang, *Principles, Introduction and Advances of Lithium Secondary Batteries*, Tsinghua University Press, Beijing (2002).
3. T. Ohzuku, Y. Iwakoshi, *J. Electrochem. Soc.*, 140 (1993) A2490.
4. P. Poizot, S. Laruelle, S. Grugeon, L. Dupont, J. M. Tarascon, *Nature*, 407 (2000) 496.
5. A. S. Arico, P. G. Bruce, B. Scrosati, J. M. Tarason, W. V. Schalkwijk, *Nat. Mater.*, 4 (2005) 366.
6. J. Chen, L. N. Xu, W. Y. Li, X. L. Gou, *Adv. Mater.*, 17 (2005) 582.
7. K. T. Nam, D. W. Kim, P. J. Yoo, C. Y. Chiang, N. Meethong, P. T. Hammond, Y. M. Chiang, A. M. Belcher, *Science*, 312 (2006) 885.
8. W. Y. Li, L. N. Xu, J. Chen, *Adv. Funct. Mater.*, 15 (2005) 851.
9. X. H. Huang, J. P. Tu, C. Q. Zhang, J. Y. Xiang, *Electrochem. Commun.*, 9 (2007) 1184.
10. P. L. Taberna, S. Mitra, P. Poizot, P. Simon, J. M. Tarascon, *Nat. Mater.*, 5 (2006) 1.
11. C. Z. Wu, P. Yin, X. Zhu, C. Z. Ouyang, Y. Xie, *J. Phys. Chem. B.*, 110 (2006) 17806.
12. P. L. Taberna, S. Mitra, P. Poizot, P. Simon, J. M. Tarascon, *Nat. Mater.*, 5 (2006) 567.
13. H. Li, P. Balaya, J. Maier, *J Electrochem Soc.*, 151 (2004) A1878.
14. J. Hu, H. Li, X. J. Huang, *Ionics*, 15 (2009) 91.
15. S. Grugeon, S. Laruelle, L. Dupont, F. Chevallier, P. L. Taberna, P. Simon, L. Gireaud, S. Lascaud, E. Vidal, B. Yrieix, J. M. Tarascon, *Chem Mater.*, 17 (2005) 5041.
16. Y. Yu, C. H. Chen, J. L. Shui, S. Xie, *Angew. Chem. Int. Ed.*, 44 (2005) 7085.
17. Y. Yu, Y. Shi, C. H. Chen, *Chem. Asian. J.*, 1 (2006) 826.
18. Y. Yu, Y. Shi, C. H. Chen, C. L. Wang, *J. Phys. Chem. C.*, 2008, 112 (2008) 4176.
19. R. Koksang, S. Yde-Andersen, K. West, B. Zachau-Christiansen, S. Skaarup, *Solid State Ionics*, 28-30 (1988) 868.
20. R. Koksang, D. Fauteux, P. Norby, K. A. Nielsen, *J. Electrochem. Soc.*, 136 (1989) 598.
21. K.-A. Wilhelmi, *Ark. Kemi.*, 26 (1966) 131.
22. R. Vidya, P. Ravindran, A. Kjekshus, H. Fjellvag, *J. Electroceram.*, 17 (2006) 15.
23. O. Chusid, E. Ein-Eli, D. Aurbach, M. Babai, Y. Carmeli, *J. Power Sources.*, 43 (1993) 47.
24. J. Jamnik, J. Maier, *Phys. Chem. Chem. Phys.*, 5 (2003) 5215.
25. P. Balaya, H. Li, L. Kienle, J. Maier, *Adv. Funct. Mater.*, 13 (2003) 621.
26. S. Laruelle, S. Grugeon, P. Poizot, M. Dollé, L. Dupont, J. M. Tarascon, *J. Electrochem. Soc.*, 149 (2002) A627.
27. Q. C. Zhuang, T. Wei, L. L. Du, Y. L. Cui, L. Fang, S. G. Sun, *J. Phys. Chem. C.*, 114 (2010) 8614.
28. X. Y. Qiu, Q. C. Zhuang, Q. Q. Zhang, R. Cao, P. Z. Ying, Y. H. Qiang, S. G. Sun, *Phys. Chem. Chem. Phys.*, 14 (2012) 2617.
29. S. Zhang, P. Shi, *Electrochim. Acta.*, 49 (2004) 1475.
30. M. D. Levi, K. Gamolsky, D. Aurbach, U. Heide, R. Oesten, *Electrochimica Acta.*, 45 (2000) 1781.